NANO LETTERS

Letter

Cite This: *Nano Lett.* 2018, 18, 5373−5381

pubs.acs.org/NanoLett

Scalable Patterning of Encapsulated Black Phosphorus

Nick Clark,[†,#] Lan Nguyen,[†,#] Matthew J. Hamer,[‡] Fredrik Schedin,[§] Edward A. Lewis,[†] Eric Prestat,[†] Alistair Garner,[†] Yang Cao,[‡] Mengjian Zhu,[‡] Reza Kashtiban,[∥] Jeremy Sloan,[∥] Demie Kepaptsoglou,[⊥] Roman V. Gorbachev,[*,‡] and Sarah J. Haigh[*,†]

[†]School of Materials, University of Manchester, Oxford Road, Manchester, M13 9PL, United Kingdom

[‡]School of Physics and Astronomy, University of Manchester, Oxford Road, Manchester, M13 9PL, United Kingdom

[§]National Graphene Institute, University of Manchester, Oxford Road, Manchester, M13 9PL, United Kingdom

[∥]Department of Physics, University of Warwick, Coventry, CV4 7AL, United Kingdom

[⊥]SuperSTEM Laboratory, STFC Daresbury Campus, Daresbury, WA4 4AD, United Kingdom

Supporting Information

ABSTRACT: Atomically thin black phosphorus (BP) has attracted considerable interest due to its unique properties, such as an infrared band gap that depends on the number of layers and excellent electronic transport characteristics. This material is known to be sensitive to light and oxygen and degrades in air unless protected with an encapsulation barrier, limiting its exploitation in electrical devices. We present a new scalable technique for nanopatterning few layered BP by direct electron beam exposure of encapsulated crystals, achieving a spatial resolution down to 6 nm. By encapsulating the BP with single layer graphene or hexagonal boron nitride (hBN), we show that a focused electron probe can be used to produce controllable local oxidation of BP through nanometre size defects created in the encapsulation layer by the electron impact. We have tested the approach in the scanning transmission electron microscope (STEM) and using industry standard electron beam lithography (EBL). Etched regions of the BP are stabilized by a thin passivation layer and demonstrate typical insulating behavior as measured at 300 and 4.3 K. This new scalable approach to nanopatterning of thin air sensitive crystals has the potential to facilitate their wider use for a variety of sensing and electronics applications.

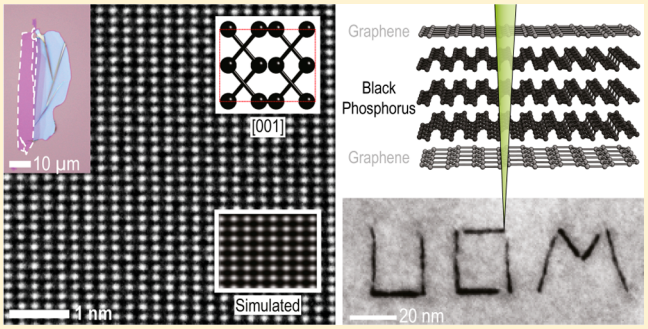

KEYWORDS: *Phosphorene, graphene encapsulation, van der Waals heterostructures, direct write oxidation, transmission electron microscopy, electron beam sculpting, local oxidation lithography*

The successful isolation of few-layer black phosphorus (BP) has generated remarkable excitement in a very short time.[1−3] Such isolation is possible due to its highly anisotropic crystal structure where corrugated layers of phosphorus atoms are bonded by weak van-der-Waals interactions and can be easily separated. Using a similar strategy to that of graphene, atomically thin layers of BP can be extracted from the bulk by mechanical exfoliation[4−6] and by liquid phase exfoliation.[7−9] As it is made progressively thinner, the direct band gap in BP varies from ∼0.3 eV in bulk to ∼1.5 eV for a monolayer.[4,10−14] Crystals only a few nanometers thick demonstrate high carrier mobility (reported hole mobility of 5200 $cm^2 V^{-1} s$ at room temperature and 45000 $cm^2 V^{-1} s$ below 20 K[15]) and high on−off ratios in field-effect devices (up to 10^5)[5,16,17] offering potential for applications in high-speed optoelectronic devices.[2,5,17−20] Black phosphorus is a complementary addition to the 2D materials library, providing a variable band gap between those of graphene (no band gap) and semiconducting 2D-dichalcogenides (which lie between 1.3 and 2 eV). Nonetheless, the exploitation of BP's electronic properties is hampered by the material's strong susceptibility to oxidation[21] in the presence of air. This degradation is amplified by humidity, exposure to light and elevated temperatures[6,22−25] leading to a drastic deterioration of BP's electronic and optical properties.[24,25] The observed degradation rate increases for thinner BP flakes,[26] with monolayers visibly degrading over the course of a few minutes and even relatively thick (10 nm) crystals degrading to form droplet-like oxidation bubbles within 24 h in air.[4,6,24,25,27] The etching process in thicker flakes (>50 nm) is observed to self-terminate after a few days due to the accumulation of oxidized phosphorus (P_xO_y) forming a protective layer on the surface of the flake.[28]

Reduced degradation of BP has been achieved using a number of different methods including deliberate generation of a protective surface oxide layer through plasma etching,[29] coating with alumina,[25,30,31] polymers,[6,30] and ionic

Received: March 8, 2018
Revised: July 27, 2018
Published: August 1, 2018

DOI: 10.1021/acs.nanolett.8b00946
Nano Lett. 2018, 18, 5373−5381

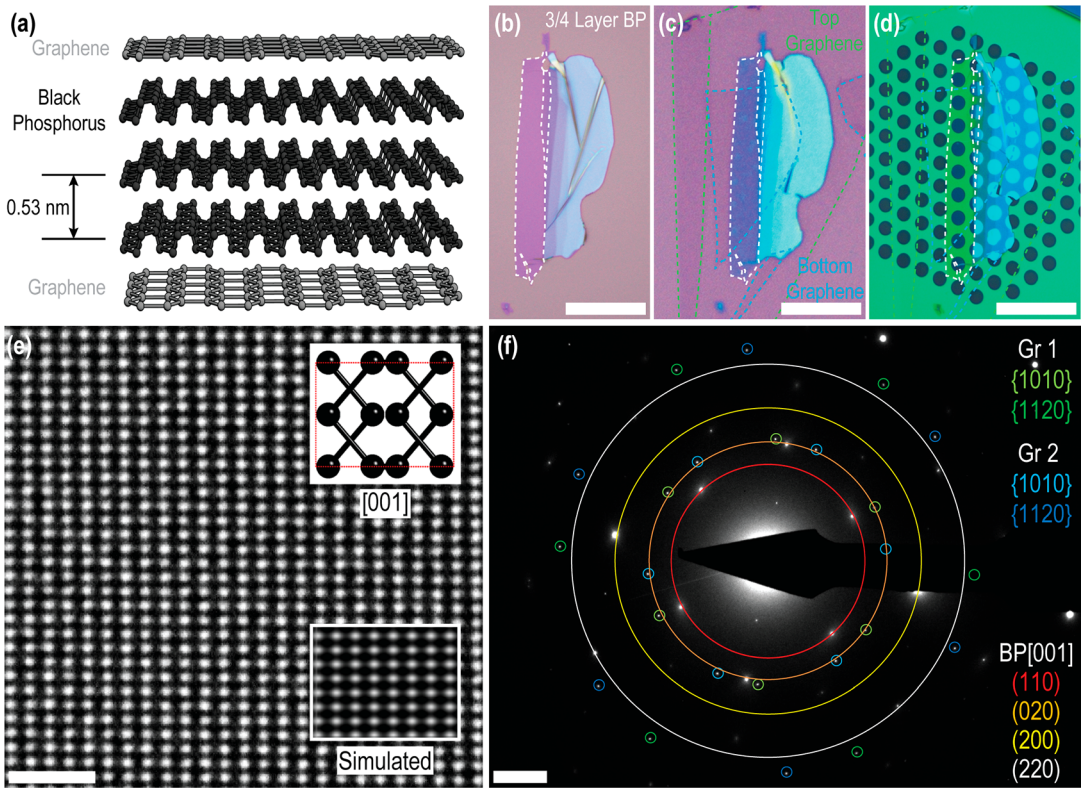

Figure 1. (a) Schematic of the graphene-encapsulated BP sample. (b) Optical micrograph of a 3−4 layer BP flake after exfoliation on an oxidized silicon substrate. (c) The same BP flake after top and bottom graphene encapsulation. The dashed lines highlight edges of mechanically exfoliated crystals. All exfoliation and transfer is performed in an argon environment glovebox to prevent oxidation of BP during the sample fabrication. (d) The same sample after transfer to a silicon nitride TEM support film. Scale bars for parts b−d are 20 μm. (e) Atomic-resolution Wiener-filtered aberration-corrected TEM image of a 5-layer thick area of pristine BP flake. The insets show an image simulation and ball-and-stick model of the [001] orientation. Scale bar is 1 nm. (f) Diffraction pattern from the area imaged in part e, showing two sets of spots corresponding to the upper and lower graphene sheets (misoriented by ∼20°), and the expected BP diffraction spots. The inner BP spots are forbidden reflections which are only visible in few-layered BP flakes (see Supporting Information, Figure S3, for diffraction pattern without overlays). Scale bar is 2 nm^{-1}.

liquids,[32,33] but perhaps the most promising method for electronic device applications is the encapsulation with 2D materials such as graphene[34] or hBN.[16,34−36] These materials provide an ultrathin, chemically robust and impermeable barrier to anything larger than a single proton.[37] Precise patterning of BP nanoribbons has been proposed as a route to tuning the band gap and electronic properties by controlling orientation, width and edge terminations.[38−42] Drndić et al.[43,44] have reported nanoscale sculpting of many-layer (17 nm thick) BP nanoribbons using direct write electron beam ablation in the STEM. Unfortunately the theoretically predicted transport properties could not be verified experimentally and the ribbon would have been susceptible to atmospheric degradation on removal from the high vacuum of the STEM.[43] Additionally, it is important to consider the potential effect of electron beam irradiation on the BP structure, both in the context of STEM patterning and for the more scalable approach of EBL processing.

Here, we develop a scalable protocol to controllably sculpt BP devices using EBL and graphene or hBN encapsulation. We demonstrate that introducing atomic scale defects in the encapsulation layer with a focused electron beam allows air species to come into contact with selected areas of the embedded BP crystal and generate a few-nanometer oxide region around the perforation point. We induce such local oxidation controllably within both STEM and EBL instruments and use electron diffraction, energy dispersive X-ray spectroscopy (EDXS), and electron energy loss spectroscopy (EELS) to study the atomic and chemical structure of the etched locations. After prolonged exposure to ambient conditions, the patterns have a smallest feature size of 6 nm (STEM) and 10 nm (EBL). Such resolution is extremely difficult to achieve using other traditional masking and etching techniques used in semiconductor fabrication due to the necessity of using polymer resists. We further show that oxidized lines as narrow as 10 nm demonstrate clear insulating behavior with a breakdown voltage well above that of vacuum even at room temperature.

Results and Discussion. The experimental BP samples were mechanically exfoliated from bulk crystals in a clean argon glovebox to avoid oxidation.[39] Thin flakes of few layer BP were identified using their optical contrast and then sandwiched between two graphene (G) or hBN crystals. For STEM experiments, monolayer graphene or hBN sheets were used to encapsulate thin (2−5 layer) BP flakes, which were then transferred to a TEM support film. The full encapsulation and transfer procedure was performed immediately after the BP exfoliation in the same argon chamber via the van der Waals pick-up technique[45,46] using our specially developed motorized micromanipulation stage.[47−49]

Figure 1b shows an optical micrograph of an exfoliated BP flake prior to encapsulation. Thin BP flakes deposited on thin thermal silicon oxide layers exhibit an enhanced optical contrast with a constant contrast difference as the layer

DOI: 10.1021/acs.nanolett.8b00946
Nano Lett. 2018, 18, 5373−5381

number is increased, making it simple to identify the number of layers in exfoliated flakes,[50] as with other 2D materials.[51,52] Parts c and d of Figure 1 show the same BP flake (from Figure 1b) after encapsulation within a G/BP/G stack on an oxidized silicon wafer and after transfer onto a silicon nitride support grid, respectively. Atomic-resolution TEM images obtained at many locations across such encapsulated crystals show the long-range pristine atomic structure of BP with no visible lattice defects in few layer crystals after 5 months of storage in air. Low magnification high angle annular dark field (HAADF) STEM images of a previously unimaged area after encapsulation for more than 6 months are included in Figure S6 in the Supporting Information. Figure 1e shows a typical TEM image where the atomic lattice is clearly visible even without filtering out the spatial frequencies of the encapsulating graphene layers. The high crystal quality of our samples is further confirmed with electron diffraction, as shown in Figure 1f. The spots marked with blue and green are the $\{10\bar{1}0\}$ and $\{11\bar{2}0\}$ reflections for two single layer graphene sheets with the upper and lower graphene lattices twisted relative to each other by ~20°. Figure 1e also contains the expected spot pattern for BP viewed along [001] where the lattice parameters are a = 3.31 Å, b = 4.38 Å, and c = 10.5 Å, as defined by Hultgren.[53] We note that other works have defined the unit cell with the b-axis being longest.[4,22,54−56] The number of layers in our BP samples can be confirmed using the ratio of the (110)/(200) spot intensities in the diffraction pattern.[4] For the sample presented in Figure 1 the ratio was found to be ~0.1, confirming that this area of BP crystal is 5 layers thick (~2.6 nm, see Figure S3 in the Supporting Information).

The encapsulated specimen area was found to be relatively robust during prolonged STEM or TEM imaging at 80 kV, while unencapsulated areas were more beam sensitive. Enhanced resistance to beam-induced damage has been previously reported in thin molybdenum disulfide (MoS_2) crystals when encapsulated by graphene.[57,58]

TEM imaging with electron energies above 80 kV is known to produce defects and holes in graphene and hBN, with both materials having similar electron beam damage thresholds.[59] Once a vacancy is formed, the under coordinated atoms surrounding the vacancy have lowered sputtering energy barriers, and are preferentially removed forming nanopores.[60] Although point defects and point defect clusters are impermeable even to molecular He, theoretical calculations have found that water and oxygen can permeate graphene and hBN when pore diameters exceed ~1 nm (as discussed in the Supporting Information, section 4). We thus propose a novel two-stage process for patterning encapsulated BP flakes using the encapsulating flake as a "resist" layer. First, a pattern is exposed using an electron beam, creating defects in the encapsulation layer. Second, the sample is exposed to air, allowing oxidizing species to penetrate through the beam-induced holes and damage the BP crystal underneath, etching it to produce the exposed pattern. In common with direct write techniques,[43] combining this approach with electron diffraction allows flake patterning to be performed along specific crystallographic directions. Black phosphorus shows strong directional anisotropy in electronic[14] and thermal[3] transport due to its ridged structure, and therefore, prior knowledge of the crystal orientation is invaluable when fabricating electronic devices to control transport behavior.

To demonstrate local etching of BP we exposed a set of 100 nm long lines into a graphene encapsulated 3 layer BP crystal

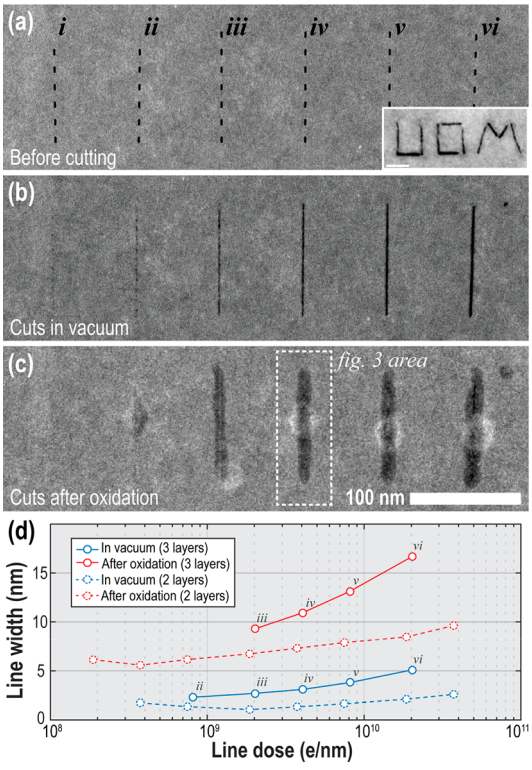

Figure 2. HAADF STEM images showing the controlled cutting of nm-resolution lines in an encapsulated (3 layer) BP flake. The width of the 100 nm long cuts is controlled by varying dwell time per pixel (i) 0.05, (ii) 0.1, (iii) 0.25, (iv) 0.5, (v) 1, and (vi) 2.5 s. Lines were drawn using a probe current of 1.3 nA, an accelerating voltage of 200 kV and 1 pixel/nm. (a) shows the area immediately prior to patterning. (b) Cuts immediately after patterning. (c) Same cuts after exposing sample to air at room temperature for 2 days. (d) Solid lines are a comparison of line widths on initial sculpting in the electron microscope (blue data) and after oxidation in air (red data) taken from the area shown in parts a−c. The dashed lines show the change in line widths in a 2 layer sample as pictured in supporting material Figure S10. The inset in part a is a demonstration of electron beam writing of "UOM" into a 10 nm thick BP crystal (scale bar: 20 nm).

using a focused STEM probe, as shown in Figure 2. By progressively increasing the electron dose used to make the cuts (pixel dwell-times varied between (i) 0.05 and (vi) 2.5 s with 100 pixels and 1.3 nA beam current, 200 kV) we change the amount of damage induced which becomes clearly visible at the dose of (iv) ~ 3×10^9 e nm^{-1} as a clear-cut approximately 3 nm wide through the entire BP film thickness. Further increase in dose leads to effective broadening of the cut up to 5 nm at 2×10^{10} e nm^{-1}.We then exposed the sample to air and ambient light for 2 days and repeated the imaging to find that the cuts have expanded laterally and had identical contrast for all exposure doses above 10^9 e nm^{-1}. The resulting line width was found to be 6−10 nm wider than before air contact giving the smallest feature size of 9 nm (for the 0.25s dwell time).

We also patterned a series of 50 nm lines on a thinner encapsulated BP crystal (2 layers), with similar line doses, as pictured in the Supporting Information, Figure S10, and achieved a smaller minimum feature size of 6 nm. The line widths are plotted along with those from the three-layer flake in Figure 2c. The difference in these two measurements could be a result of the smaller flake thickness leading to a reduction

DOI: 10.1021/acs.nanolett.8b00946
Nano Lett. 2018, 18, 5373−5381

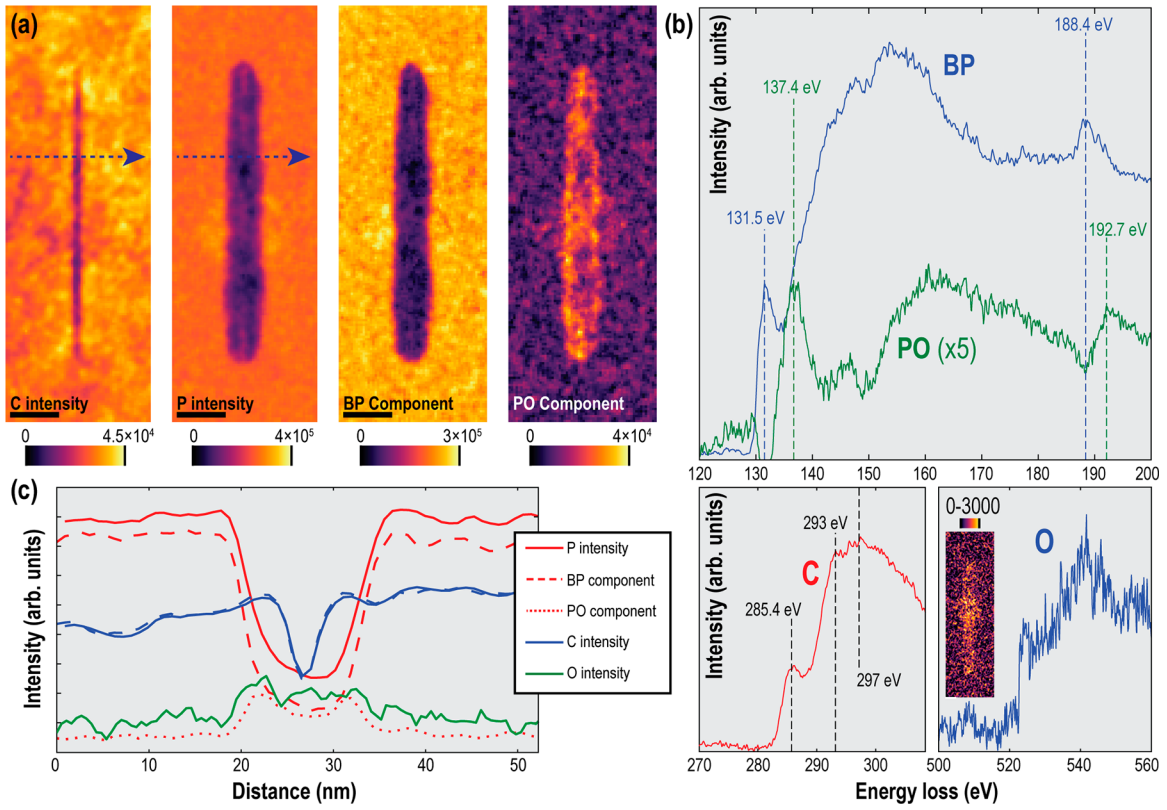

Figure 3. EEL spectrum imaging of the cut feature labeled (iv) in Figure 2c after oxidation. (a) Shows maps of the absolute intensity of the carbon K edge and the phosphorus L edges obtained by model based least-squares fitting of the spectra at every pixel, along with maps of the components of the phosphorus L edges extracted using NMF algorithm corresponding to BP and oxidized phosphorus (P_xO_y) (details of NMF decomposition in Supporting Material). Scale bars are 20 nm. (b) NMF factors corresponding to the BP and PO signals around the phosphorus L edges, as well as extracted carbon and oxygen K edges. The inset on the O K-edge plot is a map of the absolute intensity of the oxygen edge. (c) Relative elemental intensities (shown by solid lines) along the profile indicated by the dotted line in part a. The dotted lines representing the separated BP and PO components are scaled by fitting their combined intensities to the elemental P intensity.

in the electron beam spreading and a resulting decrease in the damage region for the graphene, or to differences in the passivation behavior for different BP layer thicknesses. However, we note that the difficulty of accurately focusing the electron beam prior to etching, while simultaneously minimizing imaging of the sample to prevent unwanted holes being created in the graphene sheet, could also affect the ultimate spatial resolution of the features we observe.

Importantly, the dimensions of the damaged regions were found to be stable after initial air exposure and not degrade further after several weeks' exposure to ambient conditions. This self-limiting etching behavior is likely caused by a self-passivation process and we performed chemical mapping using EEL spectroscopy to investigate this phenomena. By studying the total core-loss peak intensities, we estimate that in the center of the cut feature the carbon and phosphorus intensities are reduced to around 50% and 35% of the surrounding values respectively, indicating that most of the reaction products escape through the holes in the encapsulation layer and a relatively small amount of material is left inside of the etched volume often collecting into pockets (visible by increased contrast on Figure 2c). High resolution TEM and STEM revealed that the remaining material is amorphous and volatile on exposure to the electron beam. A similar etching methodology was applied to thicker samples and it was found to be possible to employ high beam currents to etch through the entire BP thickness even for a ∼10 nm thick specimen (the "UoM" inset from Figure 2).

One of the key advantages of this patterning technique is that above a critical threshold, the shape of the patterned BP features is mostly invariant with the line dose used to pattern the encapsulating material. Whether we have created isolated defects with a pore size >∼5 Å (cut ii in Figure 2) separated by less than a few nm, or continuously penetrated both the BP flake and encapsulating layer (e.g., cut vi in Figure 2), the self-passivating etching process means that resultant patterned BP area is remarkably similar. This means that, in contrast to conventional STEM sculpting of 2D materials,[61−63] the two-step technique can be used to consistently pattern a large area, as the patterning behavior/resultant line width (in BP) is less dependent on the local level of surface contamination or the vacuum level. This effect also helps alleviate any difference in the TEM focus across a sample; the need to prevent the "unexposed" areas from damage due to electron exposure means it is challenging to correctly focus the beam at the writing location, and minor focal differences can otherwise lead to significantly different patterning behavior. The fact that we completely penetrate through BP flakes up to 10 nm thick and their encapsulating layers (inset, Figure 2), with similar spatial resolution as for the thin flakes, implies the 2-step technique is likely to be suitable for patterning even thicker flakes.

By performing non-negative matrix factorization[64] (NMF), the EEL spectra in the region of the phosphorus L edge was

DOI: 10.1021/acs.nanolett.8b00946
Nano Lett. 2018, 18, 5373−5381

blindly separated into components corresponding to BP signals ($L_{2,3}$ onset around 132 eV, L_1 peak around 188 eV)[65,66] and oxidized phosphorus, or P_xO_y ($L_{2,3}$ onset around 137 eV, L_1 peak around 193 eV).[67] Details of the decomposition are presented in the Supporting Information, along with the individual NMF components (in Figure S12). The BP and P_xO_y characteristic spectra, and the maps of their strength, are shown in Figure 3. The P_xO_y signal is clearly maximized around the edges of the cut region, suggesting that a passivating barrier has indeed been formed. Mapping of the carbon K edge indicates that the graphene sheets have not been affected by the oxidation process, while oxygen K-edge mapping suggests an increased level of elemental oxygen in the etched region, although the signal-to-noise ratio is too low to observe increased levels around the edge, as suggested by the P_xO_y map.

The ability of the BP to form a passivating oxide barrier along the edges of the cuts has important implications. If the pattern is stable over time, we can employ the technique to define various electronic structures (e.g., transistors, quantum dots, nanoribbons, etc.) at an impressive resolution only limited by a combination of the electron probe diameter and the thickness of the passivation layer. In order for this approach to work the cuts must be electrically insulating.

To test the electrical transport properties of our patterned structures, we have produced and selectively oxidized two hBN encapsulated BP devices, with BP thicknesses of 2 and 4 layers respectively as measured using the atomic force microscope (AFM). The lower encapsulating hBN layer had a thickness of ~20 nm, and the upper hBN layer was a monolayer. After encapsulation the sample was transferred to a silicon wafer coated with a 300 nm thick thermal oxide layer, to enable electrical gating of the BP. Gold was then deposited to create high quality electrical contacts as described in our previous glovebox work.[48]

Prior to the selective oxidation process, both devices demonstrated classical field effect behavior with hole mobilities of 2000 $cm^2/(V\ s)$ and 200 $cm^2/(V\ s)$ for 4L and 2L respectively, similar to earlier reports[48,68] on encapsulated BP devices. We then used a 100 kV electron beam lithography instrument (Raith EBPG 5200) to expose narrow lines across the conductive channel as indicated by the red lines in Figure 4a,b. After the sample was exposed to ambient conditions, this exposure effectively separated contacts 2 and 3 from the rest of the device with a low bias resistivity higher than $10^8\ \Omega$, well above the $10^3\ \Omega$ value measured before the etching procedure (Figure 4c). The realistic etched line width is estimated to be 12 nm taking into account the 4 nm pattern size exposed with a 2−3 nm beam diameter and including the 6 nm oxidation broadening. It is surprising that a gap only 12 nm wide spanning across 1 μm sample size shows such a high resistivity at room temperature (reproducible in both 2L and 4L devices). Furthermore, no leakage current was observed while increasing the bias voltage up to 100 mV giving breakdown field of at least 10^7 V/m, better than that of vacuum. While the etched regions of the sample changed their conductivity dramatically, other unexposed areas (all other contacts) showed very little change, ruling out the possibility of accidental device degradation between the measurements.

While fabricating such devices it was found to be especially important to avoid any areas which had pockets of trapped contamination—a common feature seen in heterostructures fabricated by the crystal stacking technique.[47,69] In the STEM,

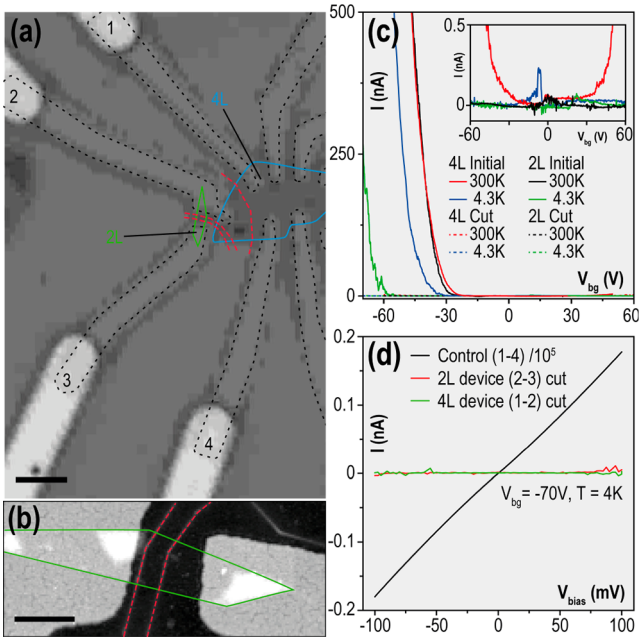

Figure 4. Electrical characterization of patterned few layer BP. (a) Optical micrograph of the device with multiple metallic contacts highlighted by black dashed line. Blue line shows edges of 4 layer BP flake (4L) and green line 2 layer BP flake (2L). Red lines indicate etched lines (b) AFM topography of the 2L device with crystal edges highlighted with green. (c) Electrical current measured in a two terminal configuration (between contacts 1−2 for the 4L flake and 2−3 for the 2L flake) before and after the etching procedure. The inset shows the dotted traces (voltages after patterning) with a reduced vertical scale to enhance visibility. (d) Current voltage characteristics measured across the 2L and 4L devices compared to unetched 4L sample (contacts 1−4). Scale bars: (a) 2 μm and (b) 500 nm.

we observed that the action of the electron beam caused such contamination bubbles to etch down through the BP crystal (Figure S4 shows growth of such a hole at a dose rate of 2500 e $nm^{-2}\ s^{-1}$). While the exact chemical composition of the trapped material inside the bubbles can vary depending on the techniques and conditions employed during the stacking procedure, we have previously shown that they contain hydrocarbon and oxygen species.[69] We hypothesize that these hydrocarbons are reduced to more chemically reactive species by the electron beam, which subsequently chemically etch the BP. After an extended period of time the etching process appears to cease, after which the holes are stable for extended periods (as shown in Figures S4 and S5, in the Supporting Information). Electron diffraction and EEL spectrum imaging of this region indicate that crystalline phosphorus is entirely absent from the center of the hole although a small amount of oxidized phosphorus remains. The encapsulating graphene layers remain intact although we cannot rule out the presence of small holes. A ring of oxidized phosphorus (P_xO_y) is seen around the edge of the hole, and outside this ring, no loss of crystallinity of the BP is observed. This suggests a similar self-passivation process to that which we observe for the etched lines, where the stable, P_xO_y, reaction product accumulates around the edge of the hole and prevents any further etching and which has been found to provide a passivation barrier for thicker BP flakes (>50 nm).[28] Similar behavior was observed in regions that had undergone high resolution TEM or STEM imaging, were then exposed to

DOI: 10.1021/acs.nanolett.8b00946
Nano Lett. 2018, 18, 5373−5381

ambient conditions for up to 2.5 months and then returned to the microscope (Figure S9 in the Supporting Information). Low dose and low accelerating voltage imaging conditions should therefore be employed to prevent the introduction of unwanted point defects while identifying the region of interest for pattern etching.

Conclusion. In conclusion, we have developed a new method for nanometer scale patterning of few-layered BP. Encapsulation with graphene or hBN is found to provide an impermeable barrier which extends the long-term stability of few-layer BP crystals from a few minutes to at least several months, protecting it from environmental oxidation caused by the presence of light, air and moisture. By selectively damaging the encapsulating layer with an electron probe the protection is locally removed and subsequent exposure to ambient conditions causes etching of the BP crystal that extends 2−3 nm from the damaged region. Importantly, the patterned features are stable and do not expand during subsequent air contact due to passivation by oxygen-containing groups. With spatial resolutions of 6 nm readily achievable in few layer BP crystals, we demonstrate that features as narrow as 10 nm are already electrically insulating. This result highlights a potential route to harnessing the exciting properties of air-sensitive crystals in real applications. Minimizing levels of trapped contamination and encapsulation with defect free graphene are likely to be critical factors for implementing this technique on a large scale and will require subsequent development of relevant fabrication and growth techniques.

Experimental Methods. *Device Fabrication.* BP samples were mechanically exfoliated from bulk crystals (supplied by HQ Graphene) in an argon filled glovebox (oxygen and water levels below 0.1 ppm) onto a thin film of polypropylene carbonate (PPC). They were then immediately encapsulated using the van der Waals pickup technique, where the top encapsulating flake (supported by a PMMA membrane) is lowered onto the chosen BP flake, and used to slowly lift it away from the PPC substrate. The stack is then lowered onto the lower encapsulating flake. For the TEM/STEM samples, monolayer graphene was used as the encapsulation material, and the stack was transferred onto a Quantifoil or silicon nitride TEM support film, before the PMMA was removed by immersion in acetone. The TEM support was then dried supercritically in a CO_2 atmosphere to prevent membrane damage due to the liquids surface tension. For the transport samples, hBN was used as the encapsulation material, with a monolayer piece on top, and a ∼20 nm thick piece below. The stack was then transferred to a 290 nm thick oxidized silicon film supported by a silicon wafer, which acted as the back gate during transport measurements. Gold contacts were then fabricated using a lift off process after mask definition using EBL. Care was taken to avoid areas where trapped contamination bubbles were observed as these features caused unwanted local BP etching.

TEM/STEM Imaging. TEM and STEM analysis of the encapsulated BP was performed with a FEI Titan 80−200 ChemiSTEM with probe-side aberration correction at 200 kV and X-FEG electron source (Figure 2, Figure 3. Figure S1−S3, S5, and S7−S9). STEM experiments were performed with a 21 mrad convergence angle probe and probe current between 75 pA and 1.5 nA. While navigating to the region of interest for etching, low probe currents, low dwell times (1 μs) and low magnification were employed to minimize unwanted irradiation damage. The HAADF detector collected electrons scattered between 48 and 191 mrad. EDX spectrum imaging was performed with a Super-X detector with a solid angle of ∼0.7 sr. EEL spectra were acquired using a GIF Quantum with an energy dispersion of 0.25 eV and a collection angle of 38 mrad, providing an effective energy resolution of 1.75 eV. Complementary EELS data was also obtained from a Nion UltraSTEM100 aberration corrected STEM operated at 60 kV with a beam current of 100 pA and showed similar features to that presented in Figure 3. The cold field emission gun had an energy spread of 0.35 eV and core loss spectrum images were acquired with a collection angle of 30 mrad. Aberration corrected TEM results were acquired on a JEOL ARM 200F at an operating voltage of 80 kV (Figure 1). The BP flakes were found to be robust to prolonged STEM imaging at 200 kV over the acquisition time of 19 s, (total dose of ∼47 e nm^{-2} with a low dose rate of 2.5 e nm^{-2} s^{-1}). The encapsulated BP crystal structure also appears stable when imaged in TEM, showing little changes even after extended atomic resolution imaging at 80 kV up to doses of 2.6×10^7 e nm^{-2} and 200 kV up to doses of 4.8×10^6 e nm^{-2}. However, imaged regions subsequently degraded when removed from the microscope vacuum, demonstrating that the graphene encapsulation had been damaged.

TEM/STEM Analysis and Simulation. Principal Component Analysis (PCA) was performed on EELS spectrum imaging data using the Hyperspy package to improve the signal-to-noise ratio.[70−72] For the EELS spectrum images shown in Figure 3, the non-negative matrix factorization (NMF) algorithm packaged in Hyperspy was run on a section of the spectrum image around the energy range of the phosphorus peak, after background removal and energy alignment using the zero loss peak. The components were then visually divided into BP and PO components (components pictured in Figure S12 in the Supporting Information), and summed to give reconstructed BP and P_xO_y spectra. For Figure S8 in the Supporting Information, multiple linear least-squares regression (MLLS) was used to separate P_xO_y and BP peaks. Both analysis approaches showed the same qualitative results. Further in depth consideration of the EELS analysis is provided in Supporting Information, section 5.

TEM image simulation was performed using the JEMS software.[73] The settings for this simulation were performed for a JEOL ARM200F with accelerating voltage = 80 kV, C_C = 1.2 mm; C_S = −0.01 mm; C_5 = 10 mm; defocus = −8 nm, and energy spread = 0.8 eV. The defocus spread was 3 nm.

Patterning Parameters. Lines were exposed in suspended graphene encapsulated hBN flakes using a FEI Titan 80−200 ChemiSTEM with a 200 kV accelerating voltage. Beam currents up to 1.3 nA were used, with a step size of 1 nm per pixel and the pixel dwell time was varied, giving total line doses between 0.2 and 2 nC/nm. For EBL thin BP areas were exposed in hBN encapsulated flakes using a 100 keV Raith EBPG 5200. A beam current of 200 pA was used, with a step size of 0.85 nm per pixel and a pattern width of 4.25 nm. The dwell time was chosen to give a total area dose of 1 C/cm^2.

■ ASSOCIATED CONTENT

Supporting Information

The Supporting Information is available free of charge on the ACS Publications website at DOI: 10.1021/acs.nanolett.8b00946.

DOI: 10.1021/acs.nanolett.8b00946
Nano Lett. 2018, 18, 5373−5381

Figures showing optical images of additional TEM samples, details of BP thickness determination using diffraction images, etching of contamination induced hole during electron illumination, low magnification images showing distribution of contamination pockets, EEL spectrum imaging of a contamination induced hole, EDX spectral imaging and selected area diffraction imaging of a BP oxidation feature caused by previous high mag STEM imaging, HAADF images of etched lines in 2 layer BP, NMF components used to separate BP and P_xO_y signals in Figure 3, EELS spectrum imaging of a wider area showing all cuts from Figure 2, and justification of choice of factor number for NMF decomposition for EEL spectrum images (PDF)

AUTHOR INFORMATION

Corresponding Authors

*(S.J.H.) E-mail: sarah.haigh@manchester.ac.uk;.

*(R.V.G.) E-mail: roman@manchester.ac.uk.

ORCID

Nick Clark: 0000-0003-3351-5628

Matthew J. Hamer: 0000-0003-3121-6536

Demie Kepaptsoglou: 0000-0003-0499-0470

Sarah J. Haigh: 0000-0001-5509-6706

Author Contributions

#N.C. and L.N. contributed equally

Author Contributions

R.V.G., Y.C., M.J.H., and N.C. made the samples. L.N., E.A.L., E.P., R.K., J.S., D.K., A.G., and S.J.H. performed the STEM experiments. R.V.G., F.S. and M.Z. performed the EBL experiments. L.N., N.C., R.V.G. and S.J.H. wrote the manuscript, and all authors contributed to analyzing the data and interpreting the results.

Funding

The authors would like to thank the Engineering and Physical Sciences (EPSRC) U.K Grants EP/G035954/1, EP/K016946/1, EP/R019428/1, EP/J021172/1, and EP/P009050/1, the NowNANO Graphene CDT, and the Defense Threat Reduction Agency Grant HDTRA1-12-1-0013 for funding. Access to aberration corrected electron microscopy was provided through the EPSRC SuperSTEM laboratory. F.S. acknowledges funding from the European Graphene Flagship Project and the European Research Council through the Hetero2D Synergy grant. S.J.H. acknowledges funding from the European Research Council (ERC) under the European Union's Horizon 2020 research and innovation program (Grant Agreement ERC-2016-STG-EvoluTEM-715502). R.V.G. acknowledges the Royal Society Fellowship scheme.

Notes

The authors declare no competing financial interest.

All raw data are available from the corresponding authors on request.

REFERENCES

(1) Churchill, H. O.; Jarillo-Herrero, P. Two-Dimensional Crystals: Phosphorus Joins the Family. *Nat. Nanotechnol.* **2014**, *9* (5), 330−1.

(2) Liu, H.; Du, Y.; Deng, Y.; Ye, P. D. Semiconducting Black Phosphorus: Synthesis, Transport Properties and Electronic Applications. *Chem. Soc. Rev.* **2015**, *44* (9), 2732−43.

(3) Ling, X.; Wang, H.; Huang, S.; Xia, F.; Dresselhaus, M. S. The Renaissance of Black Phosphorus. *Proc. Natl. Acad. Sci. U. S. A.* **2015**, *112* (15), 4523−30.

(4) Castellanos-Gomez, A.; Vicarelli, L.; Prada, E.; Island, J. O.; Narasimha-Acharya, K. L.; Blanter, S. I.; Groenendijk, D. J.; Buscema, M.; Steele, G. A.; Alvarez, J. V.; Zandbergen, H. W.; Palacios, J. J.; van der Zant, H. S. J. Isolation and Characterization of Few-Layer Black Phosphorus. *2D Mater.* **2014**, *1* (2), 025001.

(5) Li, L.; Yu, Y.; Ye, G. J.; Ge, Q.; Ou, X.; Wu, H.; Feng, D.; Chen, X. H.; Zhang, Y. Black Phosphorus Field-Effect Transistors. *Nat. Nanotechnol.* **2014**, *9* (5), 372−7.

(6) Koenig, S. P.; Doganov, R. A.; Schmidt, H.; Castro Neto, A. H.; Ozyilmaz, B. Electric Field Effect in Ultrathin Black Phosphorus. *Appl. Phys. Lett.* **2014**, *104* (10), 103106.

(7) Brent, J. R.; Savjani, N.; Lewis, E. A.; Haigh, S. J.; Lewis, D. J.; O'Brien, P. Production of Few-Layer Phosphorene by Liquid Exfoliation of Black Phosphorus. *Chem. Commun. (Cambridge, U. K.)* **2014**, *50* (87), 13338−41.

(8) Hanlon, D.; Backes, C.; Doherty, E.; Cucinotta, C. S.; Berner, N. C.; Boland, C.; Lee, K.; Harvey, A.; Lynch, P.; Gholamvand, Z.; Zhang, S.; Wang, K.; Moynihan, G.; Pokle, A.; Ramasse, Q. M.; McEvoy, N.; Blau, W. J.; Wang, J.; Abellan, G.; Hauke, F.; Hirsch, A.; Sanvito, S.; O'Regan, D. D.; Duesberg, G. S.; Nicolosi, V.; Coleman, J. N. Liquid Exfoliation of Solvent-Stabilized Few-Layer Black Phosphorus for Applications Beyond Electronics. *Nat. Commun.* **2015**, *6*, 8563.

(9) Lewis, E. A.; Brent, J. R.; Derby, B.; Haigh, S. J.; Lewis, D. J. Solution Processing of Two-Dimensional Black Phosphorus. *Chem. Commun. (Cambridge, U. K.)* **2017**, *53* (9), 1445−1458.

(10) Liu, H.; Neal, A. T.; Zhu, Z.; Luo, Z.; Xu, X.; Tomanek, D.; Ye, P. D. Phosphorene: An Unexplored 2d Semiconductor with a High Hole Mobility. *ACS Nano* **2014**, *8* (4), 4033−41.

(11) Tran, V.; Soklaski, R.; Liang, Y. F.; Yang, L. Layer-Controlled Band Gap and Anisotropic Excitons in Few-Layer Black Phosphorus. *Phys. Rev. B: Condens. Matter Mater. Phys.* **2014**, *89* (23), 235319.

(12) Das, S.; Zhang, W.; Demarteau, M.; Hoffmann, A.; Dubey, M.; Roelofs, A. Tunable Transport Gap in Phosphorene. *Nano Lett.* **2014**, *14* (10), 5733−9.

(13) Keyes, R. W. The Electrical Properties of Black Phosphorus. *Phys. Rev.* **1953**, *92* (3), 580−584.

(14) Qiao, J.; Kong, X.; Hu, Z. X.; Yang, F.; Ji, W. High-Mobility Transport Anisotropy and Linear Dichroism in Few-Layer Black Phosphorus. *Nat. Commun.* **2014**, *5*, 4475.

(15) Long, G.; Maryenko, D.; Shen, J.; Xu, S.; Hou, J.; Wu, Z.; Wong, W. K.; Han, T.; Lin, J.; Cai, Y.; Lortz, R.; Wang, N. Achieving Ultrahigh Carrier Mobility in Two-Dimensional Hole Gas of Black Phosphorus. *Nano Lett.* **2016**, *16* (12), 7768−7773.

(16) Gillgren, N.; Wickramaratne, D.; Shi, Y. M.; Espiritu, T.; Yang, J. W.; Hu, J.; Wei, J.; Liu, X.; Mao, Z. Q.; Watanabe, K.; Taniguchi, T.; Bockrath, M.; Barlas, Y.; Lake, R. K.; Lau, C. N. Gate Tunable Quantum Oscillations in Air-Stable and High Mobility Few-Layer Phosphorene Heterostructures. *2D Mater.* **2015**, *2* (1), 011001.

(17) Xia, F.; Wang, H.; Jia, Y. Rediscovering Black Phosphorus as an Anisotropic Layered Material for Optoelectronics and Electronics. *Nat. Commun.* **2014**, *5*, 4458.

(18) Buscema, M.; Groenendijk, D. J.; Blanter, S. I.; Steele, G. A.; van der Zant, H. S.; Castellanos-Gomez, A. Fast and Broadband Photoresponse of Few-Layer Black Phosphorus Field-Effect Transistors. *Nano Lett.* **2014**, *14* (6), 3347−52.

(19) Engel, M.; Steiner, M.; Avouris, P. Black Phosphorus Photodetector for Multispectral, High-Resolution Imaging. *Nano Lett.* **2014**, *14* (11), 6414−7.

(20) Low, T.; Rodin, A. S.; Carvalho, A.; Jiang, Y. J.; Wang, H.; Xia, F. N.; Castro Neto, A. H. Tunable Optical Properties of Multilayer Black Phosphorus Thin Films. *Phys. Rev. B: Condens. Matter Mater. Phys.* **2014**, *90* (7), 075434 DOI: 10.1103/PhysRevB.90.075434.

(21) Ferrari, A. C.; Bonaccorso, F.; Fal'ko, V.; Novoselov, K. S.; Roche, S.; Boggild, P.; Borini, S.; Koppens, F. H.; Palermo, V.; Pugno, N.; Garrido, J. A.; Sordan, R.; Bianco, A.; Ballerini, L.; Prato, M.; Lidorikis, E.; Kivioja, J.; Marinelli, C.; Ryhanen, T.; Morpurgo, A.; Coleman, J. N.; Nicolosi, V.; Colombo, L.; Fert, A.; Garcia-Hernandez, M.; Bachtold, A.; Schneider, G. F.; Guinea, F.; Dekker,

DOI: 10.1021/acs.nanolett.8b00946
Nano Lett. 2018, 18, 5373−5381

C.; Barbone, M.; Sun, Z.; Galiotis, C.; Grigorenko, A. N.; Konstantatos, G.; Kis, A.; Katsnelson, M.; Vandersypen, L.; Loiseau, A.; Morandi, V.; Neumaier, D.; Treossi, E.; Pellegrini, V.; Polini, M.; Tredicucci, A.; Williams, G. M.; Hong, B. H.; Ahn, J. H.; Kim, J. M.; Zirath, H.; van Wees, B. J.; van der Zant, H.; Occhipinti, L.; Di Matteo, A.; Kinloch, I. A.; Seyller, T.; Quesnel, E.; Feng, X.; Teo, K.; Rupesinghe, N.; Hakonen, P.; Neil, S. R.; Tannock, Q.; Lofwander, T.; Kinaret, J. Science and Technology Roadmap for Graphene, Related Two-Dimensional Crystals, and Hybrid Systems. *Nanoscale* **2015**, *7* (11), 4598−4810.

(22) Favron, A.; Gaufres, E.; Fossard, F.; Phaneuf-L'Heureux, A. L.; Tang, N. Y.; Levesque, P. L.; Loiseau, A.; Leonelli, R.; Francoeur, S.; Martel, R. Photooxidation and Quantum Confinement Effects in Exfoliated Black Phosphorus. *Nat. Mater.* **2015**, *14* (8), 826−32.

(23) Hanlon, D.; Backes, C.; Doherty, E.; Cucinotta, C. S.; Berner, N. C.; Boland, C.; Lee, K.; Harvey, A.; Lynch, P.; Gholamvand, Z.; Zhang, S.; Wang, K.; Moynihan, G.; Pokle, A.; Ramasse, Q. M.; McEvoy, N.; Blau, W. J.; Wang, J.; Abellan, G.; Hauke, F.; Hirsch, A.; Sanvito, S.; O'Regan, D. D.; Duesberg, G. S.; Nicolosi, V.; Coleman, J. N. Liquid Exfoliation of Solvent-Stabilized Few-Layer Black Phosphorus for Applications Beyond Electronics. *Nat. Commun.* **2015**, *6*, 8563.

(24) Island, J. O.; Steele, G. A.; van der Zant, H. S. J.; Castellanos-Gomez, A. Environmental Instability of Few-Layer Black Phosphorus. *2D Mater.* **2015**, *2* (1), 011002.

(25) Wood, J. D.; Wells, S. A.; Jariwala, D.; Chen, K. S.; Cho, E.; Sangwan, V. K.; Liu, X.; Lauhon, L. J.; Marks, T. J.; Hersam, M. C. Effective Passivation of Exfoliated Black Phosphorus Transistors against Ambient Degradation. *Nano Lett.* **2014**, *14* (12), 6964−70.

(26) Abellan, G.; Wild, S.; Lloret, V.; Scheuschner, N.; Gillen, R.; Mundloch, U.; Maultzsch, J.; Varela, M.; Hauke, F.; Hirsch, A. Fundamental Insights into the Degradation and Stabilization of Thin Layer Black Phosphorus. *J. Am. Chem. Soc.* **2017**, *139* (30), 10432−10440.

(27) Yau, S. L.; Moffat, T. P.; Bard, A. J.; Zhang, Z. W.; Lerner, M. M. Stm of the (010) Surface of Orthorhombic Phosphorus. *Chem. Phys. Lett.* **1992**, *198* (3−4), 383−388.

(28) Edmonds, M. T.; Tadich, A.; Carvalho, A.; Ziletti, A.; O'Donnell, K. M.; Koenig, S. P.; Coker, D. F.; Ozyilmaz, B.; Neto, A. H.; Fuhrer, M. S. Creating a Stable Oxide at the Surface of Black Phosphorus. *ACS Appl. Mater. Interfaces* **2015**, *7* (27), 14557−62.

(29) Pei, J. J.; Gai, X.; Yang, J.; Wang, X. B.; Yu, Z. F.; Choi, D. Y.; Luther-Davies, B.; Lu, Y. R. Producing Air-Stable Monolayers of Phosphorene and Their Defect Engineering. *Nat. Commun.* **2016**, *7*, 10450.

(30) Kim, J. S.; Liu, Y.; Zhu, W.; Kim, S.; Wu, D.; Tao, L.; Dodabalapur, A.; Lai, K.; Akinwande, D. Toward Air-Stable Multilayer Phosphorene Thin-Films and Transistors. *Sci. Rep.* **2015**, *5*, 8989.

(31) Na, J.; Lee, Y. T.; Lim, J. A.; Hwang, D. K.; Kim, G. T.; Choi, W. K.; Song, Y. W. Few-Layer Black Phosphorus Field-Effect Transistors with Reduced Current Fluctuation. *ACS Nano* **2014**, *8* (11), 11753−62.

(32) Lee, M; Roy, A. K.; Jo, S.; Choi, Y.; Chae, A.; Kim, B.; Park, S. Y.; In, I. Exfoliation of Black Phosphorus in Ionic Liquids. *Nanotechnology* **2017**, *28* (12), 125603.

(33) Chaban, V. V.; Fileti, E. E.; Prezhdo, O. V. Imidazolium Ionic Liquid Mediates Black Phosphorus Exfoliation While Preventing Phosphorene Decomposition. *ACS Nano* **2017**, *11* (6), 6459−6466.

(34) Doganov, R. A.; O'Farrell, E. C.; Koenig, S. P.; Yeo, Y.; Ziletti, A.; Carvalho, A.; Campbell, D. K.; Coker, D. F.; Watanabe, K.; Taniguchi, T.; Castro Neto, A. H.; Ozyilmaz, B. Transport Properties of Pristine Few-Layer Black Phosphorus by Van Der Waals Passivation in an Inert Atmosphere. *Nat. Commun.* **2015**, *6*, 6647.

(35) Avsar, A.; Vera-Marun, I. J.; Tan, J. Y.; Watanabe, K.; Taniguchi, T.; Castro Neto, A. H.; Ozyilmaz, B. Air-Stable Transport in Graphene-Contacted, Fully Encapsulated Ultrathin Black Phosphorus-Based Field-Effect Transistors. *ACS Nano* **2015**, *9* (4), 4138−45.

(36) Avsar, A.; Tan, J. Y.; Luo, X.; Khoo, K. H.; Yeo, Y.; Watanabe, K.; Taniguchi, T.; Quek, S. Y.; Ozyilmaz, B. Van Der Waals Bonded Co/H-Bn Contacts to Ultrathin Black Phosphorus Devices. *Nano Lett.* **2017**, *17* (9), 5361−5367.

(37) Hu, S.; Lozada-Hidalgo, M.; Wang, F. C.; Mishchenko, A.; Schedin, F.; Nair, R. R.; Hill, E. W.; Boukhvalov, D. W.; Katsnelson, M. I.; Dryfe, R. A.; Grigorieva, I. V.; Wu, H. A.; Geim, A. K. Proton Transport through One-Atom-Thick Crystals. *Nature* **2014**, *516* (7530), 227−30.

(38) Guo, H. Y.; Lu, N.; Dai, J.; Wu, X. J.; Zeng, X. C. Phosphorene Nanoribbons, Phosphorus Nanotubes, and Van Der Waals Multilayers. *J. Phys. Chem. C* **2014**, *118* (25), 14051−14059.

(39) Peng, X. H.; Copple, A.; Wei, Q. Edge Effects on the Electronic Properties of Phosphorene Nanoribbons. *J. Appl. Phys.* **2014**, *116* (14), 144301.

(40) Ramasubramaniam, A.; Muniz, A. R. Ab Initio Studies of Thermodynamic and Electronic Properties of Phosphorene Nanoribbons. *Phys. Rev. B: Condens. Matter Mater. Phys.* **2014**, *90* (8), 085424.

(41) Tran, V.; Yang, L. Scaling Laws for the Band Gap and Optical Response of Phosphorene Nanoribbons. *Phys. Rev. B: Condens. Matter Mater. Phys.* **2014**, *89* (24), 245407.

(42) Zhang, J.; Liu, H. J.; Cheng, L.; Wei, J.; Liang, J. H.; Fan, D. D.; Shi, J.; Tang, X. F.; Zhang, Q. J. Phosphorene Nanoribbon as a Promising Candidate for Thermoelectric Applications. *Sci. Rep.* **2015**, *4*, 6452.

(43) Masih Das, P.; Danda, G.; Cupo, A.; Parkin, W. M.; Liang, L.; Kharche, N.; Ling, X.; Huang, S.; Dresselhaus, M. S.; Meunier, V.; Drndic, M. Controlled Sculpture of Black Phosphorus Nanoribbons. *ACS Nano* **2016**, *10* (6), 5687−95.

(44) Cupo, A.; Masih Das, P.; Chien, C. C.; Danda, G.; Kharche, N.; Tristant, D.; Drndic, M.; Meunier, V. Periodic Arrays of Phosphorene Nanopores as Antidot Lattices with Tunable Properties. *ACS Nano* **2017**, *11* (7), 7494−7507.

(45) Pizzocchero, F.; Gammelgaard, L.; Jessen, B. S.; Caridad, J. M.; Wang, L.; Hone, J.; Boggild, P.; Booth, T. J. The Hot Pick-up Technique for Batch Assembly of Van Der Waals Heterostructures. *Nat. Commun.* **2016**, *7*, 11894.

(46) Frisenda, R.; Navarro-Moratalla, E.; Gant, P.; Perez De Lara, D.; Jarillo-Herrero, P.; Gorbachev, R. V.; Castellanos-Gomez, A. Recent Progress in the Assembly of Nanodevices and Van Der Waals Heterostructures by Deterministic Placement of 2d Materials. *Chem. Soc. Rev.* **2018**, *47* (1), 53−68.

(47) Kretinin, A. V.; Cao, Y.; Tu, J. S.; Yu, G. L.; Jalil, R.; Novoselov, K. S.; Haigh, S. J.; Gholinia, A.; Mishchenko, A.; Lozada, M.; Georgiou, T.; Woods, C. R.; Withers, F.; Blake, P.; Eda, G.; Wirsig, A.; Hucho, C.; Watanabe, K.; Taniguchi, T.; Geim, A. K.; Gorbachev, R. V. Electronic Properties of Graphene Encapsulated with Different Two-Dimensional Atomic Crystals. *Nano Lett.* **2014**, *14* (6), 3270−6.

(48) Cao, Y.; Mishchenko, A.; Yu, G. L.; Khestanova, E.; Rooney, A. P.; Prestat, E.; Kretinin, A. V.; Blake, P.; Shalom, M. B.; Woods, C.; Chapman, J.; Balakrishnan, G.; Grigorieva, I. V.; Novoselov, K. S.; Piot, B. A.; Potemski, M.; Watanabe, K.; Taniguchi, T.; Haigh, S. J.; Geim, A. K.; Gorbachev, R. V. Quality Heterostructures from Two-Dimensional Crystals Unstable in Air by Their Assembly in Inert Atmosphere. *Nano Lett.* **2015**, *15* (8), 4914−21.

(49) Bandurin, D. A.; Tyurnina, A. V.; Yu, G. L.; Mishchenko, A.; Zolyomi, V.; Morozov, S. V.; Kumar, R. K.; Gorbachev, R. V.; Kudrynskyi, Z. R.; Pezzini, S.; Kovalyuk, Z. D.; Zeitler, U.; Novoselov, K. S.; Patane, A.; Eaves, L.; Grigorieva, I. V.; Fal'ko, V. I.; Geim, A. K.; Cao, Y. High Electron Mobility, Quantum Hall Effect and Anomalous Optical Response in Atomically Thin Inse. *Nat. Nanotechnol.* **2017**, *12* (3), 223−227.

(50) Chen, H.; Fei, W.; Zhou, J.; Miao, C.; Guo, W. Layer Identification of Colorful Black Phosphorus. *Small* **2017**, *13* (5), 1602336.

(51) Blake, P.; Hill, E. W.; Castro Neto, A. H.; Novoselov, K. S.; Jiang, D.; Yang, R.; Booth, T. J.; Geim, A. K. Making Graphene Visible. *Appl. Phys. Lett.* **2007**, *91* (6), 063124.

DOI: 10.1021/acs.nanolett.8b00946
Nano Lett. 2018, 18, 5373−5381

(52) Castellanos-Gomez, A.; Agrait, N.; Rubio-Bollinger, G. Optical Identification of Atomically Thin Dichalcogenide Crystals. *Appl. Phys. Lett.* **2010**, *96* (21), 213116.
(53) Hultgren, R.; Gingrich, N. S.; Warren, B. E. The Atomic Distribution in Red and Black Phosphorus and the Crystal Structure of Black Phosphorus. *J. Chem. Phys.* **1935**, *3* (6), 351−355.
(54) Maruyama, Y.; Suzuki, S.; Kobayashi, K.; Tanuma, S. Synthesis and Some Properties of Black Phosphorus Single-Crystals. *Physica B +C* **1981**, *105* (1−3), 99−102.
(55) Shirotani, I. Growth of Large Single-Crystals of Black Phosphorus at High-Pressures and Temperatures, and Its Electrical-Properties. *Mol. Cryst. Liq. Cryst.* **1982**, *86* (1), 203−211.
(56) Morita, A. Semiconducting Black Phosphorus. *Appl. Phys. A: Solids Surf.* **1986**, *39* (4), 227−242.
(57) Zan, R.; Ramasse, Q. M.; Jalil, R.; Georgiou, T.; Bangert, U.; Novoselov, K. S. Control of Radiation Damage in Mos(2) by Graphene Encapsulation. *ACS Nano* **2013**, *7* (11), 10167−74.
(58) Algara-Siller, G.; Kurasch, S.; Sedighi, M.; Lehtinen, O.; Kaiser, U. The Pristine Atomic Structure of Mos2Monolayer Protected from Electron Radiation Damage by Graphene (Vol. 103, 203107, 2013). *Appl. Phys. Lett.* **2013**, *103* (23), 239901.
(59) Kotakoski, J.; Jin, C. H.; Lehtinen, O.; Suenaga, K.; Krasheninnikov, A. V. Electron Knock-on Damage in Hexagonal Boron Nitride Monolayers. *Phys. Rev. B: Condens. Matter Mater. Phys.* **2010**, *82* (11), 113404.
(60) Warner, J. H.; Rummeli, M. H.; Bachmatiuk, A.; Buchner, B. Atomic Resolution Imaging and Topography of Boron Nitride Sheets Produced by Chemical Exfoliation. *ACS Nano* **2010**, *4* (3), 1299−304.
(61) Borrnert, F.; Fu, L.; Gorantla, S.; Knupfer, M.; Buchner, B.; Rummeli, M. H. Programmable Sub-Nanometer Sculpting of Graphene with Electron Beams. *ACS Nano* **2012**, *6* (11), 10327−34.
(62) Fischbein, M. D.; Drndic, M. Electron Beam Nanosculpting of Suspended Graphene Sheets. *Appl. Phys. Lett.* **2008**, *93* (11), 113107.
(63) Song, B.; Schneider, G. F.; Xu, Q.; Pandraud, G.; Dekker, C.; Zandbergen, H. Atomic-Scale Electron-Beam Sculpting of near-Defect-Free Graphene Nanostructures. *Nano Lett.* **2011**, *11* (6), 2247−50.
(64) Nicoletti, O.; de la Pena, F.; Leary, R. K.; Holland, D. J.; Ducati, C.; Midgley, P. A. Three-Dimensional Imaging of Localized Surface Plasmon Resonances of Metal Nanoparticles. *Nature* **2013**, *502* (7469), 80−4.
(65) Nicotra, G.; Politano, A.; Mio, A. M.; Deretzis, I.; Hu, J.; Mao, Z. Q.; Wei, J.; La Magna, A.; Spinella, C. Absorption Edges of Black Phosphorus: A Comparative Analysis. *Phys. Status Solidi B* **2016**, *253* (12), 2509−2514.
(66) Abdolmaleki, A.; Dadsetani, M. Excitonic Effects in the K and L 2,3 Edges Spectra of Bulk and Monolayer Black Phosphorus from First-Principles. *J. Electron Spectrosc. Relat. Phenom.* **2018**, *223*, 1−10.
(67) Kruse, J.; Leinweber, P.; Eckhardt, K. U.; Godlinski, F.; Hu, Y.; Zuin, L. Phosphorus L(2,3)-Edge Xanes: Overview of Reference Compounds. *J. Synchrotron Radiat.* **2009**, *16* (2), 247−59.
(68) Chen, X.; Wu, Y.; Wu, Z.; Han, Y.; Xu, S.; Wang, L.; Ye, W.; Han, T.; He, Y.; Cai, Y.; Wang, N. High-Quality Sandwiched Black Phosphorus Heterostructure and Its Quantum Oscillations. *Nat. Commun.* **2015**, *6*, 7315.
(69) Haigh, S. J.; Gholinia, A.; Jalil, R.; Romani, S.; Britnell, L.; Elias, D. C.; Novoselov, K. S.; Ponomarenko, L. A.; Geim, A. K.; Gorbachev, R. Cross-Sectional Imaging of Individual Layers and Buried Interfaces of Graphene-Based Heterostructures and Superlattices. *Nat. Mater.* **2012**, *11* (9), 764−7.
(70) Arenal, R.; de la Pena, F.; Stephan, O.; Walls, M.; Tence, M.; Loiseau, A.; Colliex, C. Extending the Analysis of Eels Spectrum-Imaging Data, from Elemental to Bond Mapping in Complex Nanostructures. *Ultramicroscopy* **2008**, *109* (1), 32−8.
(71) Trebbia, P.; Bonnet, N. Eels Elemental Mapping with Unconventional Methods. I. Theoretical Basis: Image Analysis with Multivariate Statistics and Entropy Concepts. *Ultramicroscopy* **1990**, *34* (3), 165−78.
(72) de la Peña, F. D. L.; Ostasevicius, T.; Fauske, V. T.; Burdet, P.; Jokubauskas, P.; Nord, M.; Prestat, E.; Sarahan, M.; MacArthur, K. E.; Johnstone, D. N.; Taillon, J.; Caron, J.; Furnival, T.; Eljarrat, A.; Mazzucco, S.; Migunov, V.; Aarholt, T.; Walls, M.; Winkler, F.; Martineau, B.; Donval, G.; Zagonel, L. F.; Garmannslund, A.; Iyengar, I. Electron Microscopy (Big and Small) Data Analysis With the Open Source Software Package HyperSpy. *Microsc. Microanal.* **2017**, *23*, 214.
(73) Stadelmann, P. A. Ems - a Software Package for Electron-Diffraction Analysis and Hrem Image Simulation in Materials Science. *Ultramicroscopy* **1987**, *21* (2), 131−145.

DOI: 10.1021/acs.nanolett.8b00946
Nano Lett. 2018, 18, 5373−5381